Surface reaction of stoichiometric and calcium-deficient hydroxyapatite in simulated body fluid

J. H. CHERN LIN*, K. H. KUO†, S. J. DING, C. P. JU
Department of Materials Science and Engineering and
**Department of Mineral and Petroleum Engineering, National Cheng Kung University, 70101, Tainan, Taiwan, R.O.C.*
E-mail: chernlin@mail.ncku.edu.tw

In the present study, the immersion behavior of two kinds of sintered HA with different Ca/P ratios in two different extracellular simulated solutions (Tris buffer and Hank's solutions) was investigated and compared. Results indicated that an as-received Ca-deficient HA (FHA) had a lower Ca/P ratio, larger linear shrinkage and higher density than a stoichiometric HA (MHA). When FHA powder was calcined at 900 °C, its Ca-deficient apatite structure was unstable and a significant amount of β-TCP phase was formed. When heated to 1250 °C in air, the highly crystalline apatite structure of MHA was still stable without any noticeable decomposition. The FTIR spectra indicated that both immersed MHA and FHA in Hank's solution were gradually covered with a layer of precipitated apatite during immersion. When immersed in Tris buffer solution, neither HA showed significant changes in their FTIR spectra. SEM observation indicated that the precipitation rate on immersed FHA surface was much higher than that on MHA surface when immersed in Hank's solution. The weight loss and pH data confirmed the higher dissolution rate of FHA than MHA in Hank's solution.

1. Introduction

A variety of calcium phosphates, such as hydroxyapatite (HA, $Ca_{10}(PO_4)_6(OH)_2$), calcium pyrophosphate (DCP, $Ca_2P_2O_7$), tricalcium phosphate (TCP, $Ca_3(PO_4)_2$), and tetracalcium phosphate (TTCP, $Ca_4P_2O_9$), have been used as implant materials [1–4]. Research has shown that calcium phosphates are not only biocompatible, but highly bioactive to induce strong bonding with bone tissue [4–6]. When implanted, their surfaces are transformed into biological apatite through a sequence of reactions including dissolution, precipitation and ion exchange [1, 4]. Ideally, the resorption rate of an implant should not exceed the rate of bone formation and the resorption-induced reduction in implant strength should closely match the increase in strength of the healing tissue [5].

Among the calcium phosphate family, the popularly used HA appears to be the most biologically stable phase [5, 7]. A stoichiometric HA crystal remains structurally stable up to 1350 °C [7]. However, when an HA powder with a Ca/P ratio different from 1.67 is sintered at temperatures above 700–800 °C, its structure could be partially decomposed into TCP or TTCP [8]. TCP is generally regarded as a bioresorbable ceramic. *In vivo* test conducted by Claes *et al*. [6] showed that the volume of newly formed bone on TCP surface was higher than that on HA surface. The combination of HA and TCP, such as the so-called biphasic HA/β-TCP [9, 10], appears to be a potential candidate as implant material. This biphasic material with varying HA/β-TCP ratios could be prepared by sintering calcium-deficient apatites of varying Ca/P ratios or by sintering the mixture of HA and β-TCP [9]. It has been reported that Ca-deficient HA elicited an immediate precipitation of apatite on its surface when immersed in simulated physiological solution, whereas the precipitation on stoichiometric HA required some induction time [11]. Royer *et al*. [8] found that the flexural strength of TCP-containing HA block with a Ca/P ratio ranging between 1.60 and 1.66 was higher than that of pure HA due to the strengthening effect of TCP. It seems that Ca-deficient HA, or a biphasic HA/TCP mixture, is another potential candidate as implant material and deserves further research, such as immersion study.

A variety of synthetic solutions, such as calcium phosphate-free Tris buffer and Hank's physiological solutions, have been used for the immersion study of calcium phosphates and different results were reported [1, 12–16]. For example, Andersson *et al*. [16] found that, when their bioactive glass specimens were immersed in Tris buffer solution with citric acid, accumulation of Ca or P did not occur at the glass surface. However, when immersed in Tris buffer solution or simulated body fluid (SBF), whose composition is close to that of human blood plasma [14], a significant accumulation of Ca and P was observed.

†Corresponding author.

In the present study, the immersion behavior of two kinds of sintered calcium phosphate apatites with different Ca/P ratios (one of them is Ca-deficient and the other is stoichiometric HA) in two different extracellular simulated solutions (Tris buffer and Hank's solutions) was investigated and compared. The major techniques used for characterizing the various as-sintered as well as immersed specimens included X-ray diffraction (XRD), scanning electron microscopy (SEM) and Fourier transform infrared (FTIR) spectroscopy.

2. Materials and methods

Two commercial HA powders purchased from Merck (Darmstadt, Germany) and Ferak (Berlin, Germany) were used for the study. The compositions of these powders are listed in Table I. For simplicity, the Merck HA powder and its sintered bodies were designated as ''MHA'', while the Ferak HA powder and sintered bodies were designated as ''FHA''. As-received powders were calcined at 900 °C for 3 h, prior to sintering. For enhancing powder fluidity, both calcined powders were ball-milled in ethyl alcohol using Al_2O_3 balls and sieved through #100 mesh (325 μm). The particle size distribution of the calcined powders was determined using a laser diffraction particle size analyzer (Shimadzu, SALD-2001, Kyoto, Japan).

To determine sintering-induced green compact shrinkage, a Netzsch DIL 402 dilatometer (Netzsch Co., Tokyo, Japan) was used. In doing the tests, the calcined and sieved powder was molded in a 7 mm diameter stainless mold under a pressure of 120 MPa using a uniaxial press. The shrinkage testing was started from room temperature at a heating rate of 20 °C/min up to 1250 °C. After holding for 100 min at 1250 °C, the sintered specimens were furnace-cooled.

The various sintered specimens for immersion and other studies were fabricated as follows. The sieved powder was first pelletized to form 15 mm diameter cylinders using a uniaxial two-ended cold press at a pressure of 120 MPa. The green compacts were then heated in air to 1200 °C at a heating rate of 20 °C/min, followed by a lower heating rate of 5 °C/min up to 1250 °C. After holding for 100 min at 1250 °C, the specimens were furnace-cooled to room temperature. In an earlier report [7], it was found that the optimal sintering temperature (in terms of mechanical properties) for the Merck HA was in the neighborhood of 1250 °C. Due to shrinkage effect, the dimensions of all sintered specimens were reduced to 12.5 mm in diameter and 2 mm in thickness for immersion test. The surfaces of the specimens for immersion test were mechanically polished through 1 μm Al_2O_3 grit level. Bulk densities of sintered bodies were measured using ASTM C373-72 method [17] with Archimedes principle.

Two different extracellular solutions, Hank and Tris buffer solutions (Table II), were used for the immersion test. The commonly used Hank's solution, recommended by Pourbaix [15], has an ionic composition similar to that of human plasma. The Tris buffer solution contains only 50 mM tris(hydroxylmethyl) aminomethane and 45 mM HCl. This solution has also been widely used for the study of corrosion behavior of implant materials [1, 12, 16]. Both solutions had an initial pH of 7.4. The sintered specimens were immersed in vials containing the solution with a solution volume/sample area ratio of 10 ml/mm^2. The solution was maintained at 37 °C throughout test and was agitated daily to help maintain uniform ion concentrations. After a series of immersion times, the specimens were removed from the vials and stored in a desiccator for characterization.

Phases of the various powder and bulk specimens were analyzed using an X-ray diffractometer (Rigaku D-max IIIV, Japan) with Ni-filtered CuKα radiation operated at 30 kV and 20 mA at a scanning speed of 1°/min. An FTIR spectrometer (Nicolet 800, Nicolet Instrument Corp., Madison, WI, USA) with a resolution of 2 cm^{-1} was used to characterize the various functional groups, most importantly the hydroxyl and phosphate groups. A wavenumber range of 400–1400 cm^{-1} was selected for the analysis of immersed surfaces. In apatite structure, the phosphate group has a Td symmetry resulting in four internal modes (v1: 956 cm^{-1}, v2: 430–460 cm^{-1}, v3: 1040–1090 cm^{-1}, v4: 575–610 cm^{-1}), while the hydroxyl absorption band is located at 630 cm^{-1} (librational mode), in addition to the stretching mode at 3570 cm^{-1} [1, 11, 12]. A Hitachi S4200 SEM equipped with an energy dispersive spectrometer (EDS, NORAN, Middleton, WI, USA) was used to characterize the microstructure/microchemistry of the various powder and bulk specimens. Immersion-induced changes in solution pH value and sample weight were also determined. Prior to the weight measure using a 5-digital balance (Ael-40sm, Shimadzu, Tokyo, Japan), the immersed specimens dried at 70 °C for 24 h in an oven.

TABLE I Composition of as-received HA powders used in this study (wt %)

Composition	Merck[a]	Ferak[b]
Chloride	< 0.05	< 0.1
Fluoride	< 0.005	< 0.005
Sulfate	< 0.3	< 0.5
Heavy metals	< 0.003	< 0.003
Arsenic	< 0.0002	< 0.0002
Iron	< 0.02	< 0.04
Water	1.7	
Assay	96.5%	

[a]Merck #2196; [b]Ferak #21-735.

TABLE II Composition of extracellular solutions used in this study

Constituent	Hank* (g/L)	Tris buffer
NaCl	8.00	
$NaHCO_3$	0.35	
KCl	0.40	
$MgCl_2 \cdot 6H_2O$	0.10	
$CaCl_2$	0.14	
$Na_2HPO_4 \cdot 2H_2O$	0.06	
$MgSO_4 \cdot 7H_2O$	0.06	
KH_2PO_4	0.06	
Glucose	1.00	
$(CH_2OH)_3CNH_2$		50 mM
HCl		45 mM

*Hank's solution was adjusted to pH = 7.4 using 45 mM HCl.

3. Results and discussion

3.1. Characterization of powders and sintered bodies

The Ca/P ratios of as-received FHA and MHA powders were 1.61 ± 0.01 and 1.68 ± 0.01, respectively, as determined by EDS. The Ca/P ratio of as-received MHA powder was close to the stoichiometric Ca/P value of HA (1.67), while the lower Ca/P ratio of as-received FHA powder indicated that FHA was a calcium-deficient apatite. Both as-received powders essentially had an irregular shape and were largely agglomerated. As indicated in Fig. 1, the majority of both powders had sizes ranging from 0.5 to 5 μm. The median diameters of FHA and MHA powders were about 1.7 and 1.3 μm, respectively.

As indicated in Fig. 2, the FHA green compact started to shrink at a lower temperature and had a larger linear shrinkage than MHA compact. The final dimensional changes of FHA and MHA compacts were roughly 15.5% and 13.5%, respectively. The larger shrinkage found in FHA is possibly due to its lower activation energy for the sintering process [2]. The relative densities of MHA and FHA sintered at 1250 °C were 98.0% and 98.6% of the theoretical value of HA (3.16 g/cm^3), respectively. It is interesting that, although β-TCP has a lower theoretical density (3.07 g/cm^3) [18] than that of HA, the sintered density of β-TCP-containing FHA compact was higher than that of MHA. This might be explained by the sintering-induced shrinkage of FHA that was dominant in the determination of the final density.

XRD patterns (Fig. 3) showed that both as-received powders exhibited a relatively low crystalline apatite phase, according to JCPDS 9-432 file. As expected, after

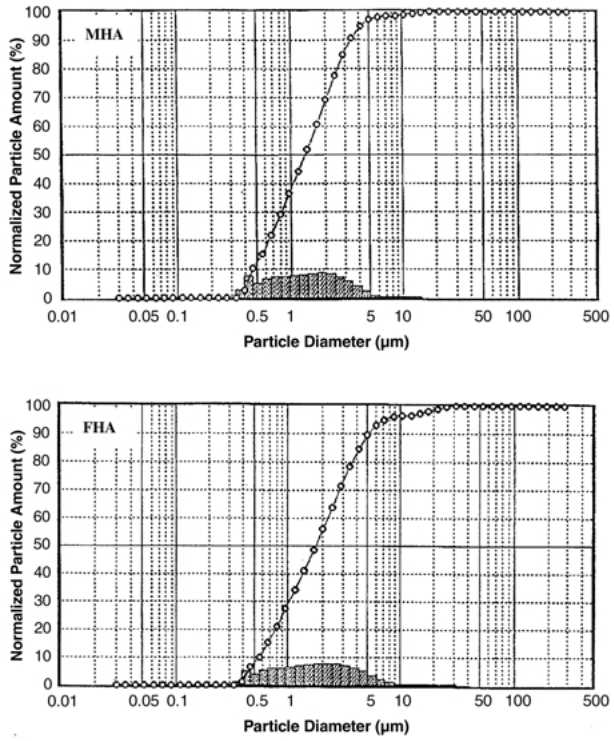

Figure 1 Particle size distribution of as-received (a) MHA and (b) FHA powders.

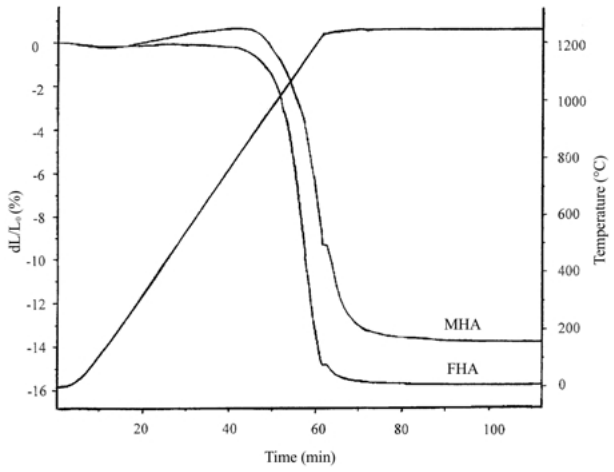

Figure 2 Linear shrinkage of MHA and FHA green compacts.

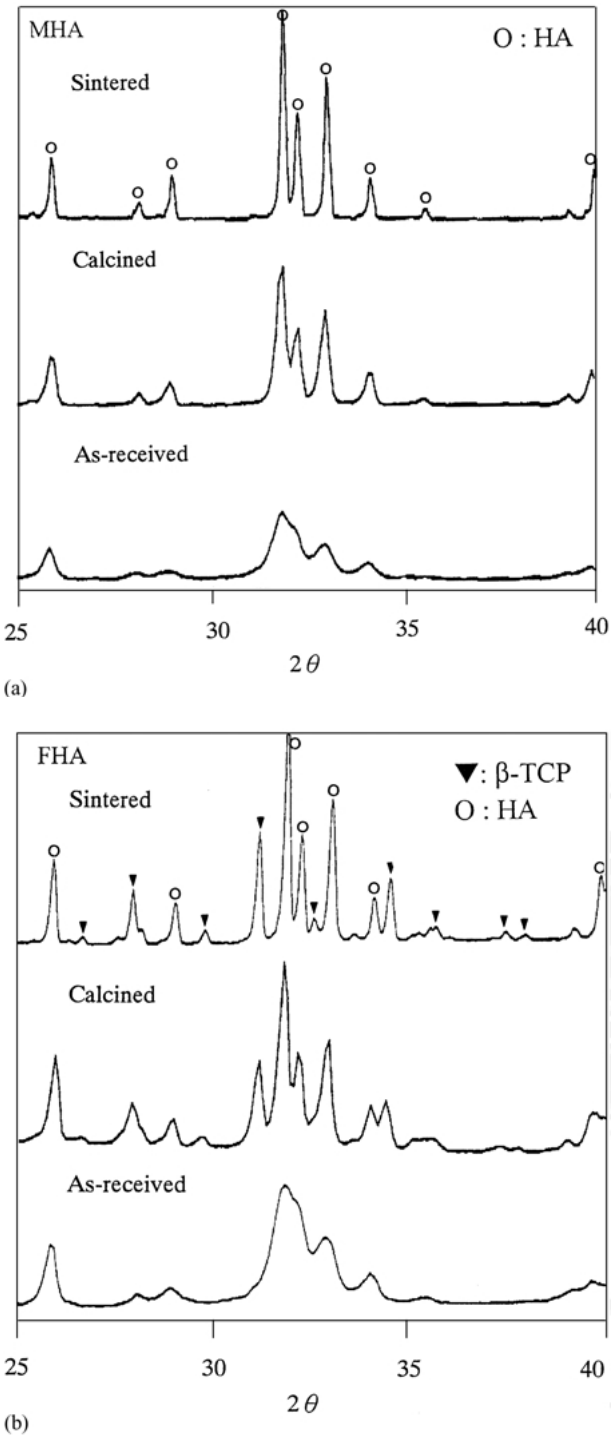

Figure 3 XRD patterns of (a) MHA and (b) FHA used in this study.

calcination at 900 °C, the crystallinity of both powders largely increased. The diffraction pattern of calcined MHA powder did not reveal any other phase than apatite. When FHA powder was calcined at 900 °C, however, its Ca-deficient apatite structure was unstable and a significant amount (roughly a half) of β-TCP phase was detected. An earlier report [19] indicated that a pyrolytic FHA powder could partially transform into β-TCP at a temperature as low as 550 °C. Compared to normal HA, the Ca-deficient FHA was easier to transform into β-TCP due to its lower Ca/P ratio. As reported previously [7, 20], the calcination treatment at 900 °C could not only cause particles to become coarser and rounder, but also increase the crystallinity level and the amount of hydroxyl functional group.

When heated to 1250 °C in air, the highly crystalline apatite structure of MHA was still stable without any decomposition, consistent with an earlier result [7]. When FHA was heated to 1250 °C, the amount of β-TCP further increased with a higher crystallinity level. Since β-TCP is biocompatible, bioactive and has been classified as a bioresorbable materials [1, 4, 6, 9, 10], the presence or dissolution of β-TCP is not expected to cause biological problems. Furthermore, when appropriately manipulated, the inclusion of this phase might provide a wide range of applications. The earlier-mentioned HA/β-TCP serve as one such example [9].

3.2. Immersion behavior of sintered bodies

3.2.1. XRD and FTIR

The XRD patterns of MHA and FHA specimens immersed in Hank and Tris buffer solutions for a series of times are shown in Figs 4 and 5, respectively. There

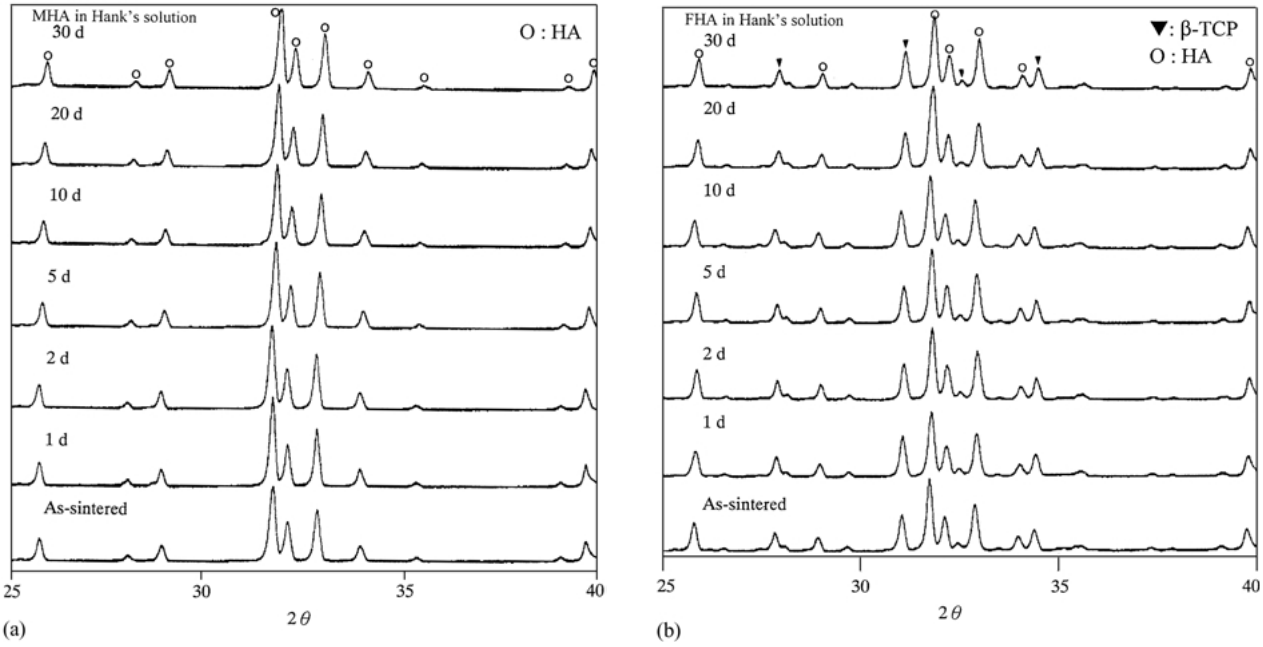

Figure 4 XRD patterns of sintered (a) MHA and (b) FHA immersed in Hank's solution.

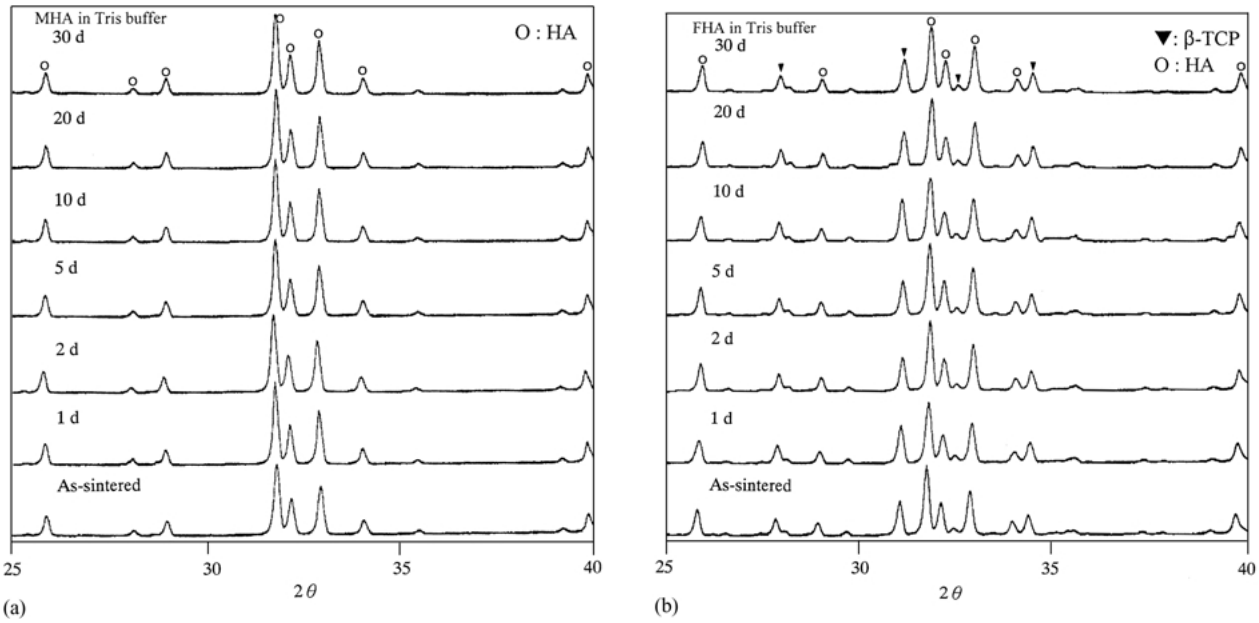

Figure 5 XRD patterns of sintered (a) MHA and (b) FHA immersed in Tris buffer solution.

were no obvious changes observed in these XRD patterns for either HA, even after immersion for as long as 30 days. It should be noted, however, that X-ray for the study could penetrate a depth of microns, even tens of microns, and is not a surface-sensitive characterization technique. The failure to see significant changes in the XRD patterns did not necessarily imply that nothing had happened at the very surface during immersion. As a matter of fact, Kokubo *et al*. [21] did detect a surface apatite layer precipitated from SBF using a grazing incidence/thin film XRD technique.

The difficulty for XRD to detect small changes on immersed surfaces was largely resolved by utilizing the more surface-sensitive FTIR technique. As shown in Fig. 6, the FTIR reflection spectrum of MHA specimen exhibited many absorption bands attributed to various functional groups. The bands at 1105, 1080, 1000, 610 and 575 cm^{-1} were attributed to PO_4 group [22]; the peak at 1130 cm^{-1} was suggested to arise from the stretching mode of HPO_4 group [23]; while the weak band at 630 cm^{-1} was derived from the vibrational modes of OH^-, indicating the presence of a dehydroxylated HA structure [22]. The slight increase in the intensity of HPO_4 absorption bands at 1130 cm^{-1} of immersed MHA in Hank's solution indicated that the MHA surface might be gradually covered with precipitated apatite during immersion [24].

The FTIR spectra of FHA before and after immersion in Hank's solution were also shown in Fig. 6. The absorption peaks at 1150, 550 and 540 cm^{-1} of as-sintered FHA were an indication of the presence of β-TCP [22, 25], consistent with XRD results. The increased intensity in absorption bands at 1125–1150 cm^{-1} of immersed FHA might be attributed to the apatite formation. When immersed in Tris buffer solution, neither HA showed significant changes in their FTIR spectra, as shown in Fig. 7.

3.2.2. SEM

As shown in Fig. 8, when immersed in Hank's solution, precipitation took place on both MHA and FHA surfaces. The amount of this precipitate, which has been identified

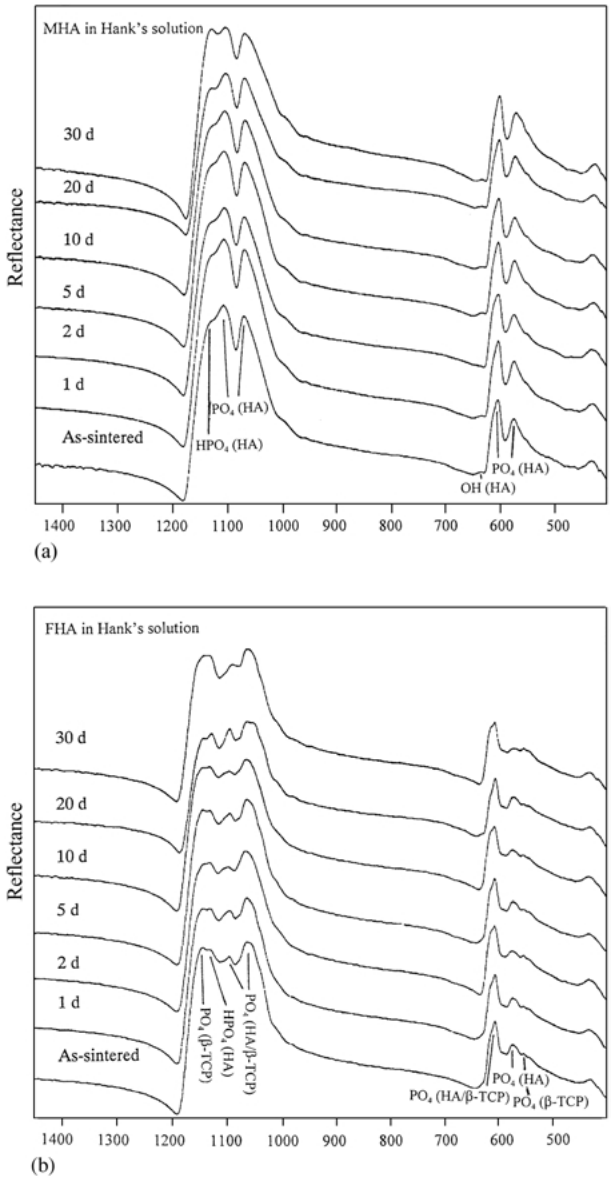

Figure 6 FTIR spectra of sintered (a) MHA and (b) FHA immersed in Hank's solution.

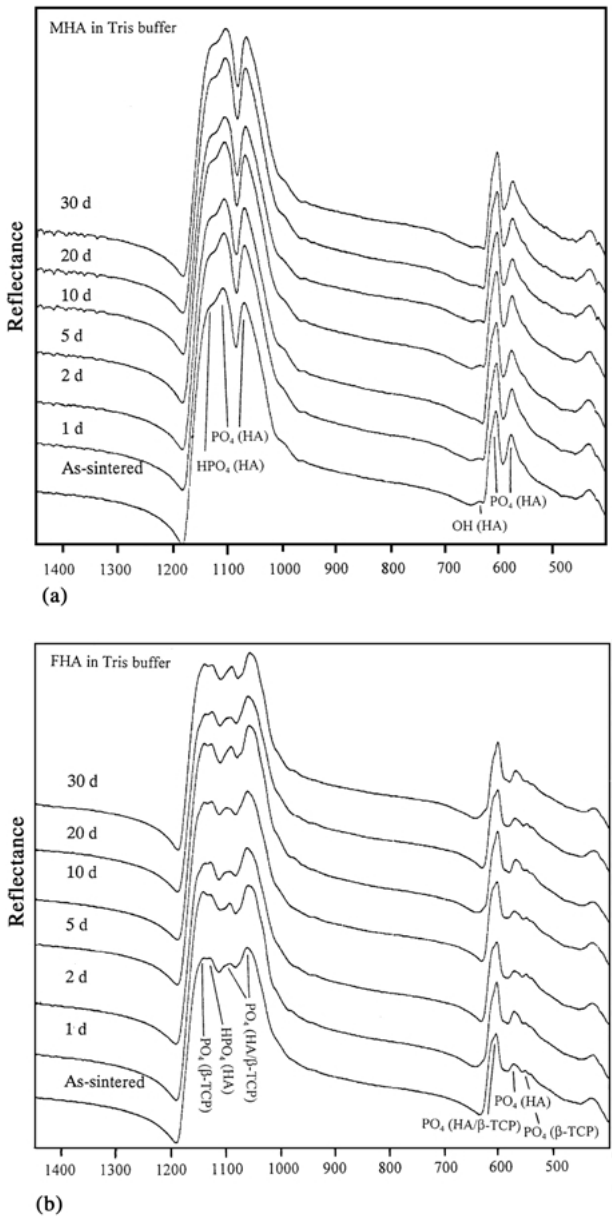

Figure 7 FTIR spectra of sintered (a) MHA and (b) FHA immersed in Tris buffer solution.

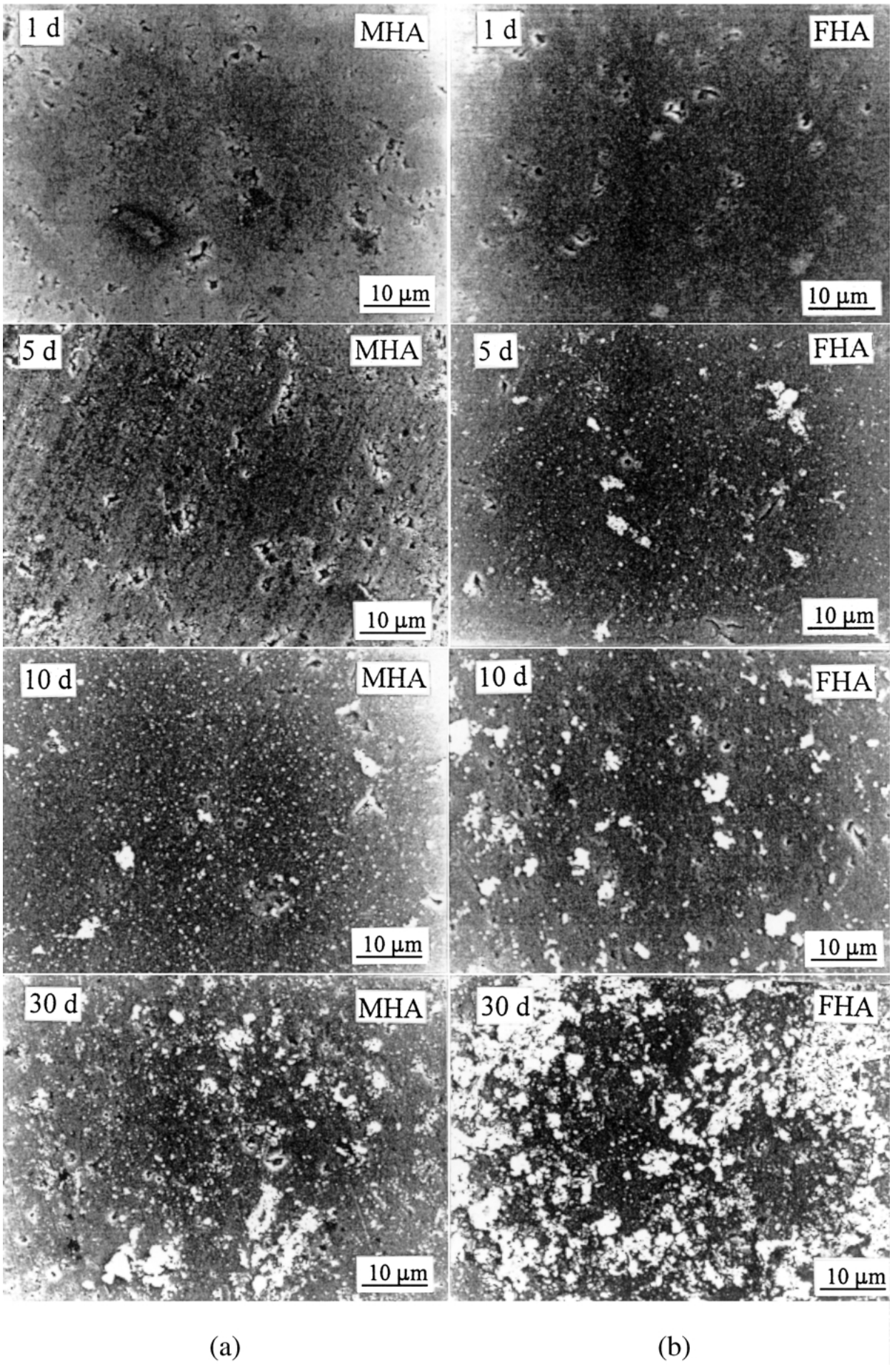

Figure 8 SEM micrographs of sintered MHA and FHA immersed in Hank's solution.

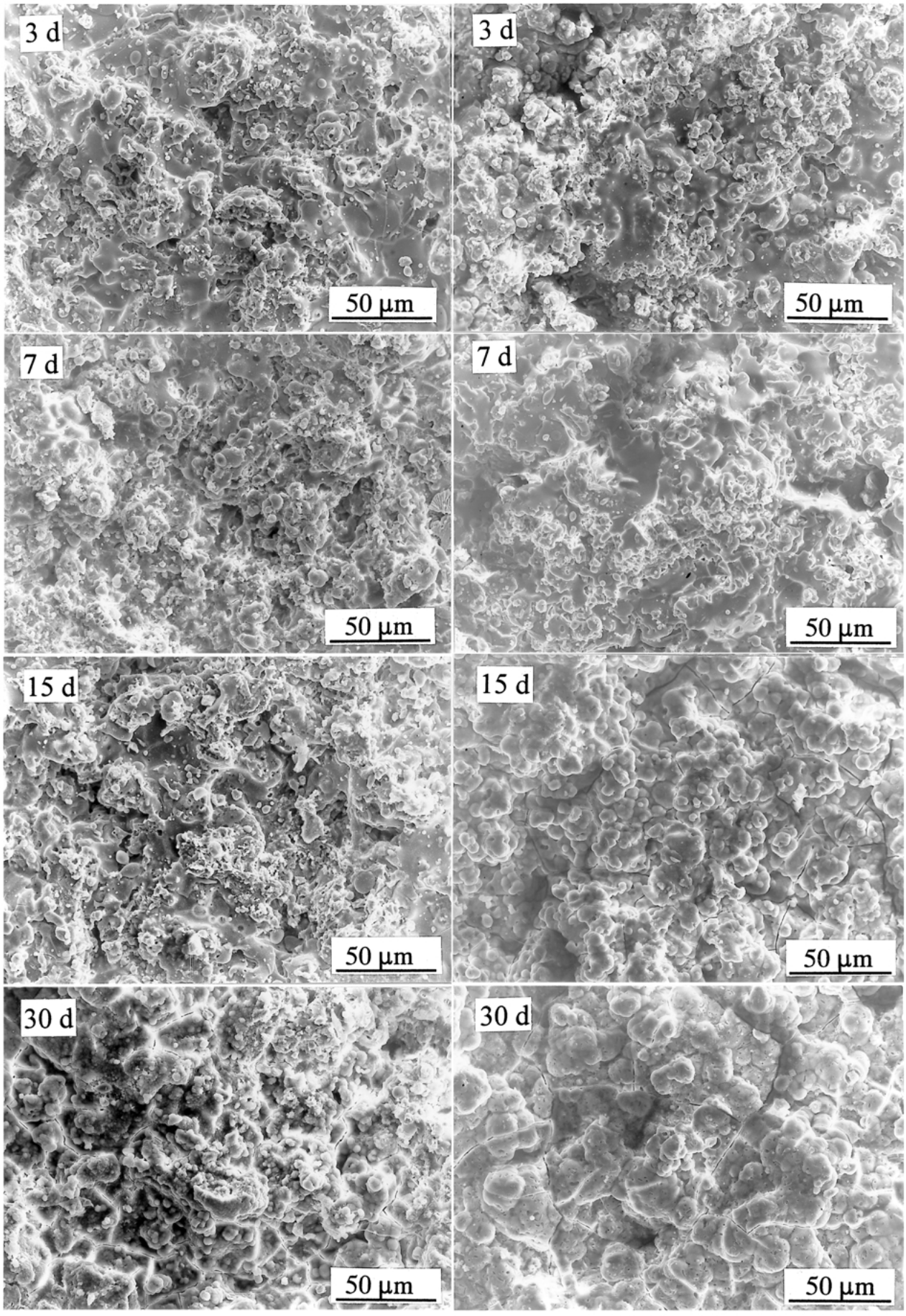

Figure 8 (Continued).

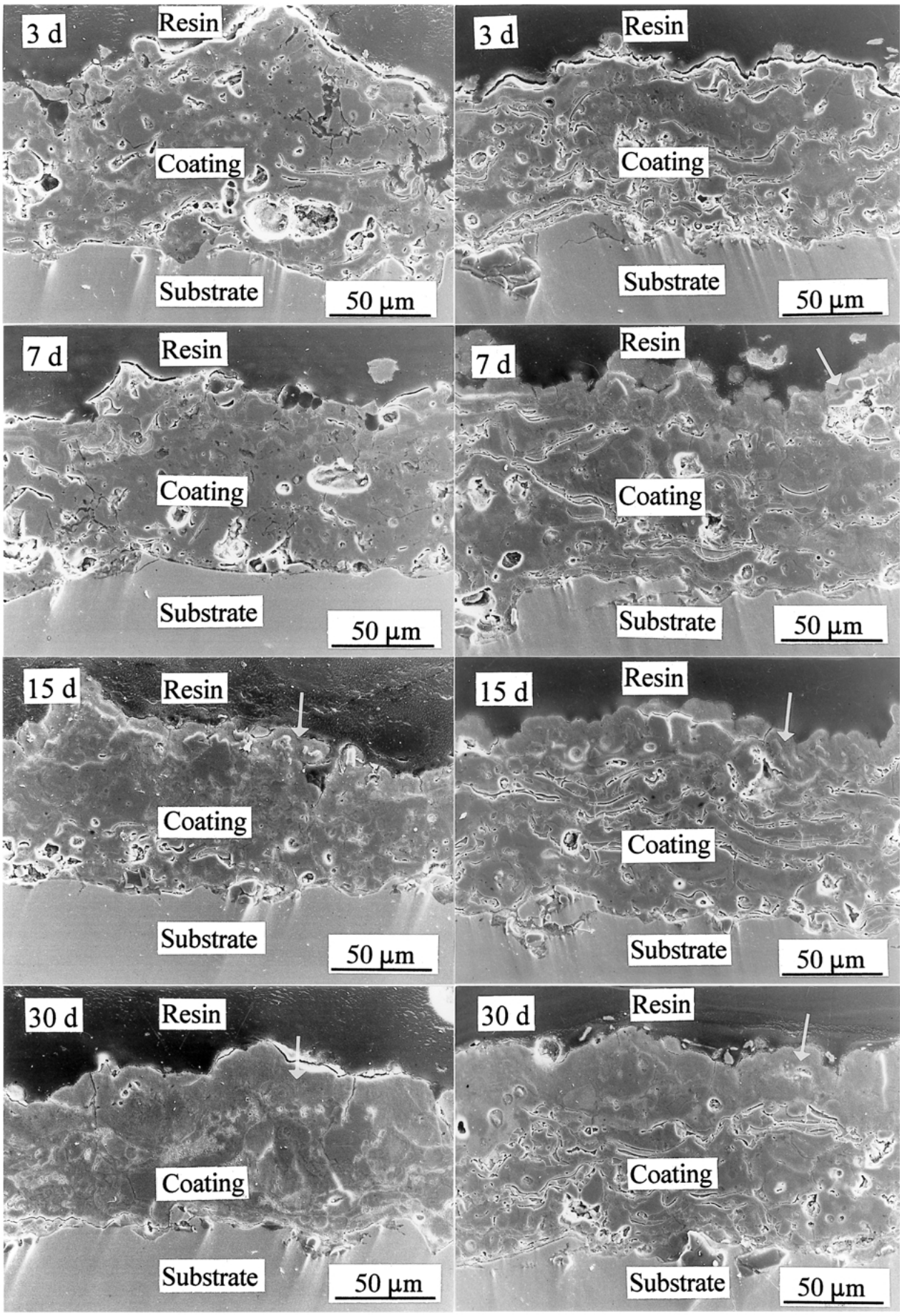

Figure 9 SEM micrographs of sintered MHA and FHA immersed in Tris buffer solution.

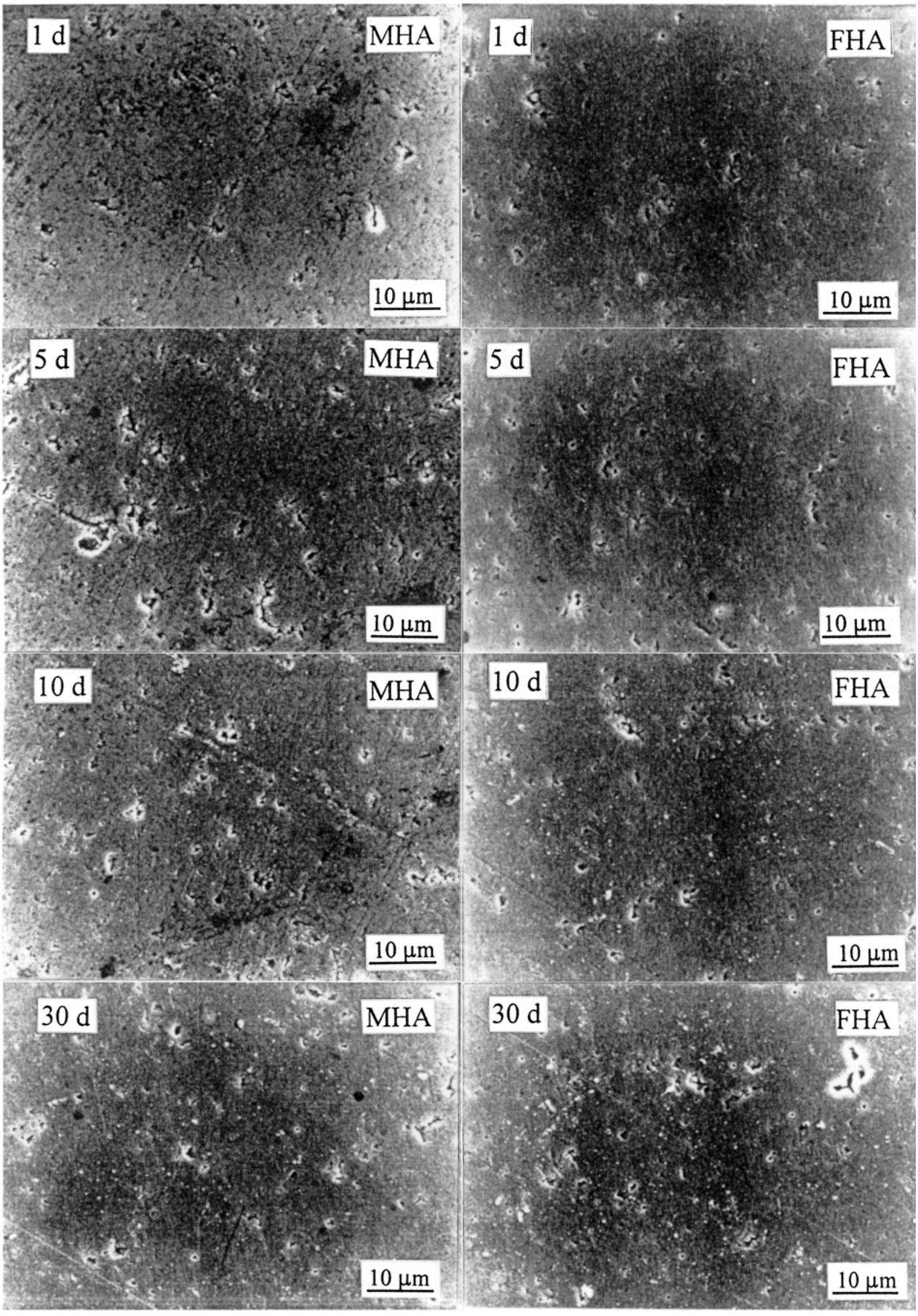

Figure 9 (Continued).

to be apatite with a Ca/P ratio of 1.6–1.8 [11, 26], increased with immersion time. This explains the earlier-mentioned changes in FTIR spectra during immersion. This apatite was formed through a sequence of reactions including dissolution, precipitation, and ion exchange [1]. According to Hench and Clark [27] and Kokubo *et al*. [21], a Ca/P-rich amorphous layer was formed *in vivo* or *in vitro* on the surface of a bioactive glass, ceramic, or glass-ceramic. This Ca/P-rich layer was later crystallized to form small carbonate-containing HA crystals. Similar apatite spherules about 2–3 μm in diameter have been observed to precipitate on bioactive glass surface immersed in SBF [16] and on plasma-sprayed HA-bioactive glass composite coatings immersed in Hank's solution [13, 26].

Although having a similar morphology, the precipitation rate on immersed FHA surface was much higher than that on MHA surface. The higher apatite precipitation rate on FHA was possibly attributed to the presence of β-TCP in FHA, which had a higher dissolution rate than HA [1, 28]. Dissolution of this β-TCP in FHA would cause an increase in calcium and phosphate ion concentrations in the solution, that, in turn, could cause a faster apatite precipitation. When immersed in Tris buffer solution, as expected, little precipitation was observed on either HA surface (Fig. 9) due to lack of necessary ions, such as Ca^{2+} and PO_4^{3-}, for the formation of apatite in the solution.

3.2.3. pH value and weight loss

When immersed in Hank's solution, both MHA and FHA samples caused pH value of the solution to increase during early stage, as shown in Fig. 10. This initial increase in pH value was a result of the dissolution of HA that released OH^- into the solution. The fact that the pH value of FHA-immersed solution increased faster than that of MHA-immersed solution provides another piece of evidence for the faster dissolution of FHA in Hank's solution due to the presence of β-TCP phase. After a few days of immersion, the pH value reached its maximum

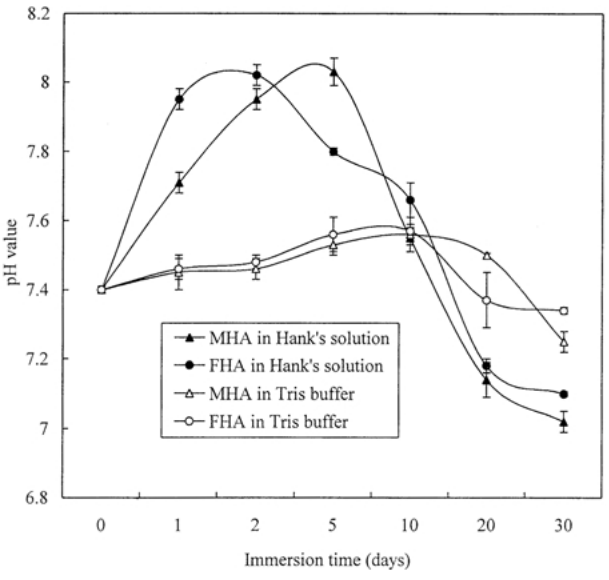

Figure 10 pH value variation during immersion.

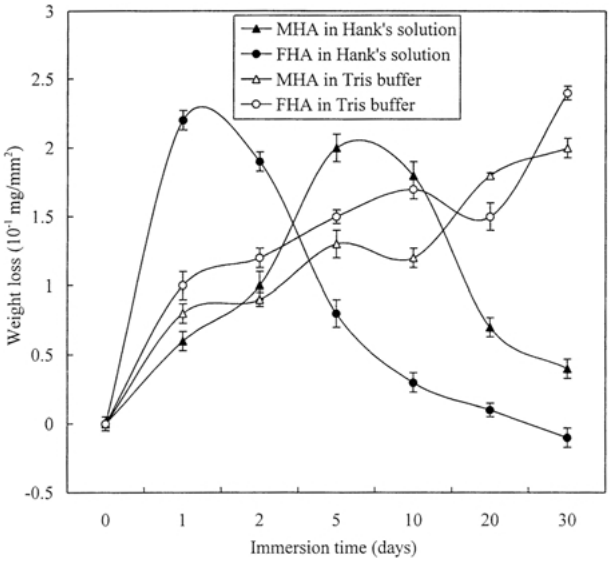

Figure 11 Weight loss variation of MHA and FHA.

(between 8.0 and 8.1), then decreased with immersion time. After 30 days of immersion, the pH values of the solutions containing MHA and FHA became 7.0 and 7.1, respectively. This decrease in pH value could be explained by the above mentioned precipitation of apatite, which consumed OH^- and/or HPO_4^{2-} in the solution [13]. When immersed in Tris buffer solution, the variations in pH value of the solution were roughly between 7.3 and 7.6 due to a buffer-mediating effect.

Consistent with pH value results, the weight losses of both HA samples first increased (dissolution), reached their maxima, then decreased (precipitation), as shown in Fig. 11. These weight loss data further confirm the higher dissolution rate of FHA in Hank's solution. As discussed earlier, this faster dissolution of FHA was due to the presence of β-TCP phase. When immersed in Tris buffer solution, both HA samples continued to dissolve without stopping (without precipitation), in agreement with all above results.

4. Conclusions

1. FHA had a lower Ca/P ratio, larger linear shrinkage and higher sintered density than those of MHA.
2. The highly crystalline apatite structure of MHA was stable without any noticeable decomposition up to 1250 °C in air. The Ca-deficient apatite structure of FHA was less stable and a significant amount of β-TCP phase was formed when heated to 900 °C.
3. Both MHA and FHA immersed in Hank's solution were gradually covered with precipitated apatite during immersion. The precipitation rate on immersed FHA surface was much higher than that on MHA surface when immersed in Hank's solution. When immersed in Tris buffer solution, neither HA showed significant changes in their XRD patterns, FTIR spectra or morphologies.
4. The pH value of FHA-immersed solution increased faster than that of MHA-immersed solution. The larger immersion-induced weight loss of FHA confirmed the higher dissolution rate of FHA in Hank's solution.

Acknowledgments

The authors acknowledge with appreciation the support for this research by the National Science Council of the Republic of China under the contract No. NSC 86-2213-E-033 & 034 & 035.

References

1. P. DUCHEYNE, S. RADIN and L. KING, *J. Biomed. Mater. Res.* **27** (1993) 25.
2. G. DE WITH, H. J. A. VAN DIJK, N. HATTU and K. PRILS, *ibid.* **16** (1981) 1592.
3. K. DE GROOT, C. P. A. T. KLEIN, J. G. C. WOLKE and J. M. A. DE BLIECK-HOGERVORST, in ''Handbook of Bioactive Ceramics'', Vol. II, edited by T. Yamamuro, L. L. Hench and J. Wilson (CRC Press, Boca Raton, FL, 1990) p. 3.
4. M. M. A. AMSELAAR, F. C. M. DRIESSENS, W. KALK, J. D. DE WIJN and P. J. VAN MULLEN, *J. Mater. Sci. Mater. Med.* **2** (1991) 63.
5. C. P. A. T. KLEIN, P. PATKA and W. DEN HOLLANDER, in ''Handbook of Bioactive Ceramics'', Vol. II, edited by T. Yamamuro, L. L. Hench, and J. Wilson (CRC Press, Boca Raton, FL, 1990) p. 53.
6. L. CLAES, H.-J. WILKE, H. KIEFER and A. MESHENMOSER, in ''Handbook of Bioactive Ceramics'', Vol. II, edited by T. Yamamuro, L. L. Hench, and J. Wilson (CRC Press, Boca Raton, FL, 1990) p. 77.
7. C. K. WANG, C. P. JU and J. H. CHERN LIN, *Mater. Chem. Phy.* **53** (1998) 138.
8. A. ROYER, J. C. VIGUIE, M. HEUGHEBAERT and J. C. HEUGHEBAERT, *J. Mater. Sci. Mater. Med.* **4** (1993) 76.
9. M. KOHRI, K. MIKI, D. E. WAITE, H. NAKAJIMA and T. OKABE, *Biomaterials* **14** (1993) 299.
10. G. DACULSI, *Biomaterials* **19** (1998) 1473.
11. S. RADIN and P. DUCHEYNE, *J. Biomed. Mater. Res.* **27** (1993) 35.
12. S. RADIN and P. DUCHEYNE, *J. Mater. Sci. Mater. Med.* **3** (1992) 33–42.
13. J. H. CHERN LIN, M. L. LIU and C. P. JU, *J. Biomed. Mater. Res.* **28** (1994) 723–730.
14. S. CHO, K. NAKANISHI, T. KOKUBO, N. SOGA, C. OHSUKI, T. NAKAMURA, T. KITSUGI and T. YAMAMURO, *J. Amer. Ceram. Soc.* **78** (1995) 1769.
15. M. POURBAIX, *Biomaterials* **5** (1984) 122.
16. O. H. ANDERSSON and I. KANGASNIEMI, *J. Biomed. Mater. Res.* **25** (1991) 1019.
17. ASTM C373-72, Annual Book of ASTM Standard, Vol. 15.02 (1982) p. 182.
18. J. D. SANTOS, J. C. KNOWLES, R. L. RIES, F. J. MONTEIRO and G. W. HASTINGS, *Biomaterials* **15** (1994) 5.
19. K. H. KUO, C. Y. HUANG, J. H. CHERN LIN and C. P. JU, 1997 Annual Symposium of the Ceramics Society, Tainan, Taiwan, ROC, 1997, p. 72.
20. J. H. CHERN LIN, H. J. CHEN and C. P. JU, *J. Dent. Res.* **72** (1993) 1364.
21. T. KOKUBO, S. ITO, Z. T. HUANG, T. HAYASHI, S. SAKKA, T. KITSUGI and T. YAMAMURO, *J. Biomed. Mater. Res.* **24** (1990) 331.
22. B. O. FLOWLER, E. C. MORENO and W. E. BROWN, *Arch. Oral Biol.* **11** (1966) 477.
23. J. ARENDS, J. CHRISTOFFERSEN, M. R. CHRISTOFFERSEN, H. ECKERT, B. O. FLOWLER, J. C. HEUFHEBAERT, G. H. NANCOLLAS, J. P. YESINOWSKI and S. J. ZAWACKI, *J. Crystal Growth* **84** (1987) 515.
24. M. REGINA, T. FILGUEIRAS, G. LA TORRE and L. L. HENCH, *J. Biomed. Mater. Res.* **27** (1993) 1485.
25. T. R. N. KUTTY, *Indian J. Chem.* **8** (1970) 655.
26. S. J. DING, C. P. JU and J. H. CHERN LIN, *J. Mater. Sci. Mater. Med.* in press, 1999.
27. L. L. HENCH and A. E. CLARK, in ''Biocompatibility of Orthopaedic Implants'', Vol. 2, edited by D. F. Williams (CRC Press, Boston, 1982) p. 129.
28. C. P. A. T. KLEIN, A. A. DRISSEN and K. DE GROOT, *Biomaterials* **5** (1984) 157.

Received 4 January
and accepted 28 July 2000